

# Tar Yield and Collection from the Pyrolysis of Large Biomass Particles

R. S. MILLER and J. BELLAN *Jet Propulsion Laboratory, California Institute of Technology, Pasadena, CA 91109-8099*

*(submitted June 28, 1996)*

**ABSTRACT**— Tar yield and collection from the pyrolysis of relatively large particles of biomass are investigated using the model of Miller and Bellan (1996b). A variety of feedstocks are considered by varying the ratios of cellulose, hemicellulose and lignin within the biomass. Effects of secondary tar reactions, quenching, temperature, particle size and carrier gas are assessed. Secondary tar reactions occurring in both the particle's interior and the exterior boundary layer strongly reduce the potential amount of tar available for collection compared to the maximum given by kinetic predictions. The primary effect of these reactions is the existence of an optimal reactor temperature range for maximizing tar yields. This range is a function of both the quenching location and the initial particle size. For rapid quenching near the particle surface, tar collection is maximized at high temperatures for small particles, and at low temperatures for large particles. For delayed quenching, low temperatures slow the secondary reactions and provide larger tar yields for all particle sizes investigated. Tar yields are also dependent on the choice of the inert carrier gas; primarily due to changes in heat capacity. A sensitivity study is performed in order to assess the influence of the biomass apparent density, thermal conductivity, heat capacity and primary heats of reaction,

*Key words:* biomass, modeling, porous particle, pyrolysis, tar, wood

## NOMENCLATURE

$C$	Specific heat.
$d$	Characteristic pore length scale.
$D$	Molecular species diffusivity.
$e$	Specific internal energy.
$K$	Reaction rate.
$M$	Molecular weight.
$N$	Total number of species.
$p$	Pressure.
$r$	Radial coordinate.
$R$	Radial position.
$\tilde{R}$	Universal gas constant.

$\dot{S}$	Reaction source/sink term.
$t$	Time.
$T$	Temperature.
$u$	Gas phase velocity.
$X$	Char formation mass ratio for reaction $K_3$ .
$Y$	Gas phase mass fraction.

### *Greek Symbols*

$\Delta h$	Heat of reaction.
$\varepsilon$	Porosity.
$\nabla$	Divergence of the velocity.
$\lambda$	Thermal conductivity.
$\mu$	Molecular viscosity.
$\rho$	Apparent density.
$\hat{\rho}$	True density.
$\sigma$	Stefan-Boltzmann constant
$w$	Emissivity.

### *Subscripts and Superscripts*

$o$	Initial value.
$c$	Conversion.
$eff$	Effective.
$g$	Gas phase.
$H$	Harvest.
$i$	Species $i$ .
$R$	Reactor.
$s$	Solid phase.
$t$	Total (all species and phases).
$T$	Thermal.
$v$	Constant volume.
$l$	Excluding char.

## 1 INTRODUCTION

The efficient extraction of condensable tar vapors from commercial biomass pyrolysis reactors is relevant to many technologies. Diebold and Powers (1988) discussed the potential commercial applications of biomass tars for use in resins and adhesives. More recently, Chornet *et. al.* (1992) addressed the feasibility of fast pyrolysis processes for the large scale harvesting of tar oils from crude biomass for hydrogen fuel production. Chornet *et. al.* (1992) suggested that it may be possible to obtain up to 75% of weight conversion to liquid yields and described techniques for conversion to hydrogen. Although the usefulness of tar oils is well accepted, optimal reactor designs for oil extraction are not established. Fluidized bed and entrained flow reactors have received major attention (Scott *et. al.*, 1988) due to both their potential for scaling to commercially relevant capacities, and to widespread previous hydrodynamic studies (e.g. Lim *et. al.*, 1995). Other reactor designs under investigation include the rotating cone (Wagenaar *et. al.*, 1992) and the cylindrical vortex (Diebold and Powers, 1988) reactors both of which use centrifugal acceleration of biomass particles against a heated wall for rapid heat transfer. Reactors designed for tar collection generally operate at moderate temperatures ( $\sim 800K$ ) as secondary tar decomposition reactions are observed to dominate at larger temperatures. It is also recognized that rapid quenching of the pyrolysis vapors can be used to minimize the extent of secondary reactions in order to improve the oil yields. However, results obtained for the cylindrical vortex reactor are so far limited to bench scale reactors and greater understanding of collection methodology is necessary before a commercially successful scaleup is attempted.

Most of the previous scientific investigations of biomass pyrolysis are limited to the study of residual mass as related to charcoal production (see e.g. DiBlasi, 1993b for a recent review). Liquid and/or gas yields have not only been studied much less, but the studies have also been restricted primarily to very small, kinetically controlled particle sizes. Turner and Mann (1981) present experimental measurements from the pyrolysis of oak particles with mean size  $< 1\text{ mm}$  at relatively mild temperatures  $< 675K$ . Reported tar yields at intermediate times show peak values of  $\approx 50\%$  by mass whereas at later times, the yields are observed to decrease, indicating the presence of secondary tar decomposition reactions. Scott and Piskorz (1982) and Scott *et. al.* (1988) studied maple particles with mean size  $\sim 100\mu m$  and report maximum tar yields  $> 80\%$  by mass at moderate reactor temperatures of  $\approx 775K$ . These large yields were the result of the small particle size and rapid quenching of the pyrolysis vapors. Liden *et. al.* (1988) developed a kinetics model incorporating secondary tar reactions to explain these results. The proposed reaction scheme suggests that primary tar yields increase monotonically with increasing reaction temperatures, but that competing secondary tar decomposition dominates at large temperatures, therefore resulting in an optimal temperature range for collection.

Unfortunately, the grinding of biomass to kinetically controlled sizes is relatively expensive and commercial processes necessarily entail relatively large, diffusion limited particle pyrolysis (e.g. Antal, 1982). In contrast to tar resulting from particles pyrolyzing in the kinetically controlled region, the tar produced from large particles

may exhibit prolonged tar residence times inside the biomass particle. Thus, secondary tar decomposition in these regions may significantly reduce the available tar yields and cannot be overcome by improved quenching methods. This effect was observed in the numerical simulations of a 2.5 cm thick wood slab at large reactor temperatures performed by DiBlasi (1993a) who showed that tar yields collected at the particle surface are increased by more than a factor of two by turning off the secondary reactions. These simulations which include secondary reactions indicate tar yields < 20% by mass; much less than observed for kinetically controlled pyrolysis. The DiBlasi model does not, however, consider the exterior particle boundary layer where further reactions occur and hence cannot account for the associated effects inherent in tar collection in real reactors. Furthermore, Miller and Bellan (1996a) showed that the kinetics employed in DiBlasi (1993a) are incapable of predicting experimentally observed pyrolysis behavior. In contrast, the new kinetics of Miller and Bellan (1996b) combined with the porous particle model of Miller and Bellan (1996a) predicted results which agree favorably with observations from a large variety of biomass pyrolysis experiments. Their particle pyrolysis model includes full property variations, thermal and mass boundary layer effects, and accounts for feedstock variations through superimposed cellulose, hemicellulose and lignin kinetics. An important prediction from the model is the existence of an optimal temperature regime for tar production.

The objective of this paper is to present results relevant to tar yield optimization from biomass pyrolysis of relatively large particles. Efforts are focused on particles sizes  $\sim 1\text{ cm}$  in order to illustrate the effects of pyrolysis on typical waste wood chips potentially used in commercial applications. Although results are obtained only for spherically symmetric and isolated particles in initially quiescent environments, implications for large scale reactor design are discussed where appropriate. The macro-particle model of Miller and Bellan (1996b) is used to simulate the pyrolysis of a variety of biomass feedstocks. Of particular interest are the effects of secondary tar reactions, quenching, particle size, reactor temperature and the choice of an inert carrier gas on the tar yield. In addition, an analysis is performed illustrating the sensitivity of several important biomass properties. The paper is organized as follows: Section 2 presents a summary of the pyrolysis model. Section 3 addresses the simulation results for a variety of biomass feedstocks and pyrolysis conditions as related to tar yields. Section 4 is devoted to conclusions and further discussions.

## 2 PYROLYSIS MODEL

The macro-particle pyrolysis model has been described in detail in Miller and Bellan (1996b) and is therefore only summarized here. The kinetics scheme for the model is based on superimposed CELLULOSE, hemicellulose and lignin reactions. In this manner, any biomass feedstock can be simulated through the knowledge of its initial mass composition with respect to these three primary components. Each of the virgin components undergoes an initial

depolymerization reaction:



This is followed by two primary competing compositions, ns, to tar



and to a combination of char and gas:



Secondary tar decomposition is also modeled as a single step irreversible reaction:



All reactions are modeled with first order Arrhenius kinetics. The frequency factors and activation energies for reactions  $K_1$ ,  $K_2$ ,  $K_3$  and the mass ratio  $X$  are all dependent on the particular biomass component, whereas all heats of reaction and secondary tar decomposition parameters are independent of the source component. Reaction  $K_1$  has  $Ah_1 = 0$ , reaction  $K_2$  is endothermic with  $\Delta h_2 = 255 \text{ kJ/kg}$ , and both the char formation and secondary tar reactions are exothermic with  $\Delta h_3 = -20 \text{ kJ/kg}$  and  $\Delta h_4 = -42 \text{ kJ/kg}$ . All remaining parameter values are provided in Miller and Bellan (1996b).

The porous particle model incorporates all property variations, is valid both inside and outside the particle, and employs a fully transient momentum equation in contrast to the traditional use of the empirical Darcy's Law. The derivation of the model has been addressed previously in Miller and Bellan (1996a) and only the final general form of the equations (in spherically symmetric coordinates) is presented here:

$$\frac{\partial \rho_{s,i}}{\partial t} = \dot{S}_{s,i}, \quad (5)$$

$$\frac{\partial \rho_g}{\partial t} + \frac{1}{r^2} \frac{\partial}{\partial r} (r^2 \rho_g u) = \dot{S}_g, \quad (6)$$

$$\frac{\partial \rho_g Y_i}{\partial t} + \frac{1}{r^2} \frac{\partial}{\partial r} \left( r^2 \rho_g Y_i u - r^2 \rho_g D_{eff}^{(i)} \frac{\partial Y_i}{\partial r} \right) = \dot{S}_{g,i}, \quad (7)$$

$$\frac{\partial \rho_g u}{\partial t} + \varepsilon \left[ \frac{\partial}{\partial r} (\rho_g u^2) \right] = -\frac{\partial p}{\partial r} + \frac{1}{r^2} \frac{\partial}{\partial r} \left[ r^2 \mu_{eff} \left( 2 \frac{\partial u}{\partial r} - \frac{2}{3} II \right) \right] + \frac{4}{3} \frac{\mu_{eff} II}{r} - 4 \frac{\mu_{eff} u}{r^2}, \quad (8)$$

$$\frac{\partial c_t}{\partial t} + \frac{1}{r^2} \frac{\partial}{\partial r} \left[ r^2 c_g u - r^2 \lambda_{eff} \frac{\partial T}{\partial r} \right] = p II + \sum \dot{S}_i \Delta h_i, \quad (9)$$

$$p = \frac{\rho_g}{\varepsilon} \left( \sum Y_i / M_i \right) RT, \quad (10)$$

where

$$\rho_g = \rho_{fig}, \quad \rho_{s,i} = (1 - \varepsilon) \hat{\rho}_{s,i}, \quad \varepsilon = 1 - \sum_s \rho_{s,i} / \hat{\rho}_{s,i}, \quad (11)$$

$$D_{eff}^{(i)} = \varepsilon D^{(i)}, \quad \mu_{eff} = \varepsilon \sum_{i=1}^g Y_i \mu^{(i)}, \quad (12)$$

$$\lambda_{eff} = (1 - \varepsilon) \left\{ \frac{\sum_{i=1}^s \rho_i \lambda^{(i)}}{\sum_{i=1}^s \rho_i} + \frac{\sigma d T^3}{\omega} \right\} + \varepsilon \sum_{i=1}^g Y_i \lambda^{(i)}, \quad (13)$$

and

$$c_g = \rho_g \left( \sum_{i=1}^g C_v^{(i)} \right) T, \quad c_s = \left( \sum_{i=1}^s \rho_{s,i} C^{(i)} \right) T, \quad c_t = c_g + c_s. \quad (14)$$

All properties are provided in Miller and Bellan (1996b). Previous comparisons with a large variety of experiments for different biomass feedstocks were favorable, particularly for small particle sizes ( $< 1 \text{ cm}$ ). Deviations from experimental observations for large particles were associated with differences in the particle geometry between the experiment and model, and with the identical set of properties used for all biomass components and types. Thus, the only difference in the calculations for different feedstocks is in the mass compositions of cellulose, hemicellulose and lignin. The lack of experimental data characterizing biomass components and types is addressed here through a sensitivity study.

### 3 RESULTS

The configuration considered is that of a single isolated and spherically symmetric biomass particle in an initially quiescent environment composed of a super-heated and inert carrier gas. The outer boundary of the computational domain is chosen to be at  $R_R = 10R_{p,0}$ , the thermal radius is  $R_T/R_{p,0} = 5$  ( $R_T$  is defined such that the temperature is held constant at  $T = T_R$  for all positions  $r \geq R_T$ ) and 96 numerical grid points are used for all simulations. The entire domain  $r \leq R_R$  is resolved in the simulations in order to account for secondary tar reactions and their effects on pyrolysis evolution. All simulations are for constant reactor temperatures, atmospheric pressure, and a uniform initial particle temperature  $T_{p,0} = 300 \text{ K}$ . Boundary conditions, the numerical method, and a discussion of effects of the above parameters are provided in Miller and Bellan (1996a). The carrier gas is chosen to be steam (unless otherwise noted) due to its attractiveness for commercial applications (see Table 1 for carrier gas properties used in this work). All simulations are terminated when the particle mass achieves 99.9% conversion (denoted as the conversion time,  $t_c$ ).

In biomass reactors, the pyrolysis vapors are typically quenched in order to cool the tar oils and thereby minimize the extent of secondary tar decomposition. However, it is expected that some decomposition will occur within the boundary layer exterior to the particle. This process was well understood by Scott *et al.* (1988) who used rapid quenching to maximize tar yields. In order to address the effects of quenching in the current simulations, an effective “harvest radius” ( $R_H$ ) is employed to define the maximum normalized “tar collection” available at location  $R_H$ :

$$\text{Tar Collection} = \frac{\int_0^{t_c} 4\pi R_H^2 \cdot \rho_g Y_{tar} u \cdot dt}{\int_0^{\infty} 4\pi r^2 \rho_s(t=0) \cdot dr} \quad (15)$$

where all variables in the numerator are evaluated at  $r = R_H$ , and the denominator is the initial particle mass. With this definition, the tar collection corresponds to the normalized mass of tar passing through the radial position  $R_H$  ( $R_{p,0} \leq R_H \leq R_R$ ) integrated over the entire duration of the simulation. Thus, the tar collection at small  $R_H$  corresponds to rapid quenching with minimal secondary tar reactions *in the* boundary layer, whereas large  $R_H$  values indicate minimal quenching conditions. The derived tar collection is not an exact representation of achievable yields as tar remaining inside the region  $r < R_H$  (in particular inside the particle) at the final simulation time  $t = t_c$  is not included. The value of studying the radial dependence of the tar collection is to provide insight into the relative effects of quenching secondary tar reactions in the boundary layer upon attainable tar yields during pyrolysis.

Figure 1 presents the variation in biomass pyrolysis behavior for a variety of feedstocks. The conversion is defined as  $(1 - \% \text{ char formed})$  and the tar collection is defined by Eq. (15). The simulated particles have initial size  $R_{p,0} = 0.5 \text{ cm}$ , the reactor temperature is  $T_R = 900 \text{ K}$  and the tar collection is evaluated at the particle surface ( $R_H = R_{p,0}$ ). All mass compositions of the biomass components are provided in Table 2. Initial heating of the particle from room temperature requires  $\approx 60 \text{ s}$  before significant pyrolysis occurs. The plots are all extended to  $t = 250 \text{ s}$ , past the conversion time, in order to clarify the differences among feedstocks. The conversion variable is observed to behave similarly to the surface tar collection. High lignin content biomass (e.g. olive husk) tends to produce large char yields and therefore low relative tar collections. In contrast, the largest tar collections are produced by the high cellulose content beech and pine woods. Significant deviations in final char yields are observed for the various feedstocks ranging over approximately 10% of the initial particle mass. However, the absolute variation in tar yield is not strongly dependent on the particular biomass (approximately 3% range) and may be smaller than experimental uncertainty for tar measurements. This is due to the large particle size which allows considerable secondary reactions to occur within the particle. Note that the tar yields are in all cases  $< 20\%$  by mass, much less than the sub-millimeter sized particles used in the experiments of Scott *et al.* (1988). The remaining discussions are primarily for maple which represents a typical hardwood, and/or for olive husk representing a high-lignin content feedstock.

### 3.1 Effects of Secondary Reactions and Quenching

The dramatic limitations imposed on the potential tar collection by finite particle sizes and secondary reactions are illustrated in Fig. 2 where the kinetic limits of char and tar production for both maple and olive husk (secondary reactions turned off) are plotted. Theoretically, almost the entire particle mass can be converted into tar at large temperatures. However, several factors present during realistic pyrolysis strongly reduce these potential yields. First, the secondary reactions which occur both inside and outside the particle convert tar to gas at rates which increase exponentially with temperature. Large particles are characterized by longer tar residence times in the

particle's interior, hence more time for secondary reactions to occur. Second, endothermic reactions and diffusion limitations result in "effective pyrolysis temperatures" significantly below the reactor temperature for finite particle sizes. Therefore, real particles pyrolyze in a relatively low temperature range in which tar production is reduced. This latter effect is discussed in detail in Miller and Bellan (1996a) and Miller and Bellan (1996b).

An additional constraint on the actual tar collection in a reactor is introduced by the method of pyrolysis vapor quenching. As pyrolysis proceeds, pressure builds within the particle resulting in tars and gases ejected into the particle's surroundings which is typically at temperatures large enough to induce further secondary tar reactions. It is therefore desirable to quench these reactions as rapidly as possible in order to maximize the actual collected tar oils. Figure 3 depicts the normalized tar collection evolution for various harvest locations. The results for maple are under the same conditions as those of Fig. 1. The maximal tar collection is at the particle surface, corresponding to a perfectly efficient quenching process. As quenching becomes less efficient, the tar collection is strongly reduced. Under the present conditions, only negligible tar yields are observed for  $R_H \geq 5R_{p,0}$ . In addition, the maximal tar yield is less than 20% of the initial particle mass; this is significantly less than the kinetic limits shown in Fig.2. These results clearly indicate the importance of the quenching process for reactors which aim at maximizing tar collection.

### 3.2 Effects of the Reactor Temperature and the Initial Particle Size

Several effects of the reactor temperature are addressed in Fig. 4 which depicts both the final char yield and the final tar collection magnitudes for both maple and olive husk. The curves are produced using results at  $t=t_c$  from eleven different simulations for each feedstock. The initial particle size is  $R_{p,0}=0.5cm$ . As discussed above, the observed variation in char yield among the feedstocks is much larger than for the tar collection; the reduced difference between tar collection for different feedstocks is due to secondary reactions. Note also that the final char yield dependence on temperature is markedly reduced from the kinetic limits observed in Fig.2 due to endothermicity and associated effective pyrolysis temperature effects. In fact, a comparison with the char yield limits in Fig.2 suggests that the effective pyrolysis temperature is  $< 650K$  for all reactor temperatures considered for this particle size. This behavior is in agreement with previous observations of Narayan and Antal (1996); Miller and Bellan (1996a); Miller and Bellan (1996b) and helps to explain the markedly reduced tar yields obtained for large particle sizes (as discussed above).

The most striking feature of Fig.4 is the presence of maximum tar collection magnitudes for moderate reactor temperatures when the quenching is relatively rapid ( $R_H \leq 1.5R_{p,0}$ ). As was described above, although larger primary tar production occurs for increasing temperatures (see Fig.2), corresponding increases in the secondary reaction rates are in competition with this process. Therefore, an optimal pyrolysis temperature for tar collection may exist, depending on the efficiency of the quenching process. As quenching becomes less efficient, the optimal



pyrolysis temperature decreases and tar collection becomes a decreasing function of  $T_R$ . The existence of optimal temperatures for tar collection is confirmed by past maple wood pyrolysis observations of Scott and Piskorz (1982) and Scott *et.al.* (1988). Although in these experiments, only very small particle sizes ( $\sim 100\mu m$ ) were investigated, the optimal reactor temperature was observed to be  $\approx 775K$  which is in good agreement with the current results.

The initial particle size is also expected to influence tar collection from biomass pyrolysis by altering the tar residence time inside the particle. This effect is highlighted in Fig.5 for three different reactor temperatures and three different harvest radii. In all cases, tar collection is observed to decrease with increasing particle size at constant temperature. This result is independent of the harvest radius and is due to an increase in the tar residence time inside of the particle. For collection locations relatively far from the particle surface ( $R_H \geq 1.5R_{p,0}$ ), the tar collection decreases with increasing reactor temperature within the range considered. This is again due to the corresponding increased secondary tar decomposition for large temperatures.

The most interesting feature of Fig.5 is the observed crossing points for the tar collection for small harvest radii, corresponding to rapid quenching. In these cases (Fig.5a and Fig.5b), the optimal reactor temperature for tar production is a function of the particle size. For small particles  $\sim 1mm$ , tar residence times are decreased and the tar collection is governed predominantly by the primary production reaction; therefore, maximal collections are observed at large reactor temperatures. However, as the particle size increases, along with tar residence times, secondary tar decomposition dominates at high temperatures. This results in desirable lower reactor temperatures for tar collection.

### 3.3 Effects of the Carrier Gas

All of the above results were obtained using steam as an inert gas; however, in many experiments nitrogen is used to purge tar from the particles and make it available for collection (e.g. Scott *et.al.*, 1988). Figure 6 illustrates the effect of the carrier gas by comparing the pyrolysis of maple wood using both steam and nitrogen as inert gases, under otherwise identical conditions. The initial particle size is  $R_{p,0} = 0.5cm$  and the reactor temperature is  $T_R = 900K$ . Figure 6a depicts the mass averaged particle temperature:

$$\langle T \rangle = \frac{\int_0^\infty 4\pi r^2 \rho'_s T \cdot dr}{\int_0^\infty 4\pi r^2 \rho'_s \cdot dr}, \quad (16)$$

as a function of normalized time. The mass averaging is with respect to the solid phase species, neglecting the char contribution, and this parameter has been discussed previously in Miller and Bellan (1996a) and Miller and Bellan (1996b). The primary difference between the two carrier gases affecting the present results is in the magnitude of the specific heat capacity (see Table 1) which is more than 2.5 times larger for steam. The associated larger specific internal energy of the steam results in an increased “thermal mass” for heat exchange with the

particle. Therefore, the maple sample in the steam environment is heated to, and reacts at, higher temperatures than the same sample in a nitrogen environment (Fig.6a). As discussed above, the larger reaction temperature causes an associated decrease in the tar collection when rapid quenching is performed. The small reversal in trends observed at  $R_H = 2R_{p,0}$  is related to the far field temperature exterior to the particle. q-bus, care must be taken in extrapolating any results to different reactor conditions. Nevertheless, the primary influence by the inert gas on pyrolysis is through its heat capacity and corresponding changes in the effective reaction temperature.

### 3.4 Sensitivity Analysis

The above particle pyrolysis calculations were performed by using the same set of properties for all biomass species. The only difference between feedstocks is their composition in terms of mass percentages of cellulose, hemicellulose and lignin. In their current form, the calculations are made for identical properties and heats of reaction for all three of the primary biomass components (cellulose, hemicellulose and lignin). In addition, these properties and heats of reaction are assumed to be independent of the source feedstock. This is the result of very limited data available regarding these properties, making it impossible to tailor their values for each component and/or feedstock. Miller and Bellan (1996b) suggested that observed deviations between the model predictions and experimental results for large ( $> 1\text{cm}$ ) particles may be attributed to the lack of specificity in property values; particularly to the assumed feedstock independence. In order to determine the importance of these effects on tar collection, a sensitivity study of several of the assumed biomass thermal properties is made. In particular, the biomass apparent density, thermal conductivity  $\gamma$ , heat capacity and primary heats of reaction are investigated.

Figure 7 compares the effects of the initial apparent density of the biomass on the temporal evolution of the tar collection at several harvest radii. All simulations are for pine wood with  $R_{p,0} = 0.5\text{cm}$  and  $T_R = 900\text{K}$  and the tar collection values are for various harvest radii,  $R_H/R_{p,0}$ . The base value for the calculations is  $\rho_w = 650\text{kg/m}^3$  which was taken from experimental hardwood measurements made by Koufopoulos et. al. (1991). However, this value may be too large for softwoods and other biomass feedstock. For example, Pyle and Zaror (1984) presented experimental measurements in the range  $[450\text{kg/m}^3, 550\text{kg/m}^3]$  for pine wood. In fact, the deviations found in Miller and Bellan (1996b) for large particles were for pine wood pyrolysis comparisons. These deviations were attributed primarily to the predicted pyrolysis initialization being longer than observation. Figure 7 shows that these deviations may be attributed to the apparent density. Lower values of the density result in earlier pyrolysis initialization; however, the final tar yields are not altered significantly. Therefore, care should be taken in prescribing the apparent density for softwoods and other feedstocks, particularly when temporal evolutions are of interest.

Figure 8 presents the temporal evolution of the tar collection from maple wood as a function of both the biomass thermal conductivity and heat capacity. In all cases, the initial particle size is  $R_{p,0} = 0.5\text{cm}$ ,  $T_R = 900\text{K}$ , and the

tar collection is at the particle surface ( $R_H = R_{p,0}$ ). Three values for each parameter are chosen, including the base value. Figure 8a shows that neither a 25% increase or decrease in the thermal conductivity significantly alters the tar collection. **Increases** in the conductivity allow larger particle/reaction temperatures and result in larger tar yields *at the particle surface* (see Fig. 5a). On the other hand, tar collection is particularly sensitive to changes in the heat capacity by as little as  $\pm 10\%$  (Fig. 8b). Large heat capacities initially cause delayed heating of the particle due to increased thermal inertia. However, at later times during the reaction, the larger heat capacities result in an increased resistance to endothermic cooling and therefore are characterized by a larger reaction temperature. These competing effects cause the curve crossing at intermediate times in Fig. 8b and result in the increasing final tar collections with heat capacity.

The final parameters for sensitivity investigation are the heats of reaction for the primary pathways  $K_2$  and  $K_3$ . Effects of these parameters on the tar collection evolution are depicted in Fig. 9 for the same particle conditions as in Fig. 8. In both cases, the heat of reaction is altered by  $\pm 20\%$ . The sensitivity of the endothermic heat of reaction is not substantial as observed in Fig. 9a. increasing the magnitude of  $\Delta h_2$  decreases the particle and reaction temperature; this correspondingly decreases the tar collection at the surface of the particle as discussed above. The three curves for various values of  $\Delta h_3$  (char production reaction) almost completely overlap (Fig. 9b). This is because at high temperatures the primary tar reaction dominates over the char production reaction; particularly when weighted by the heat of reaction. At lower reactor temperatures, such as those employed for charcoal production, it is expected that changes in  $\Delta h_3$  will have a greater impact than changes in  $\Delta h_2$ .

#### 4 CONCLUSIONS

Tar yields and collection from relatively large particles have been predicted using the detailed biomass pyrolysis model of Miller and Bellan (1996b). The numerical results were obtained for spherically symmetric particles in initially quiescent environments. Results for a variety of biomass feedstocks, including several hardwoods, softwoods, olive husk and wheat straw indicated that the absolute deviation among feedstocks is more significant for char yields than for the mass of tar oils available for collection. This was attributed to prolonged residence times and secondary tar reactions occurring inside of the particles.

The results also show that the competing processes of primary tar production and secondary tar decomposition interact in different ways depending on the particular set of pyrolysis conditions. In particular, secondary tar reactions can occur both in the particle's interior and in the exterior boundary layer. Interior reactions become important when the tar residence time is large, whereas outer reactions are primarily important when the pyrolysis vapors are not rapidly quenched near to the particle surface. In either case, the potential tar collection is greatly reduced relative to the kinetic limits for realistic finite particle sizes. In addition, as the quenching process

becomes less efficient due to the secondary reactions, tar collection is substantially reduced from that exiting the particle surface.

An important result which is conceptually applicable to reactor design is the existence of an optimal reactor temperature for maximizing the tar collection; this optimal temperature is the direct result of the competing tar reactions discussed above. For particle sizes  $\sim 1\text{ cm}$ , the optimal temperature was observed to be  $\approx 875\text{ K}$  for efficient quenching near the particle surface. This result is in good agreement with Scott *et al.*'s (1988) past experiments in a bench scale fluidized bed reactor. Tar collection is a strong function of the initial particle size; predominantly due to alterations in tar residence times. The optimal reactor conditions for tar production are highly dependent on the particle size: The simulations show that when quenching is efficient, tar collection increases for small particles ( $\sim 1\text{ mm}$ ) with increasing reactor temperature; however, larger particles ( $\sim 1\text{ cm}$ ) show the opposite behavior with temperature. For poor quenching (far from the particle surface) decreasing tar yields are obtained with increasing temperature for all particle sizes considered.

In addition to reactor temperature, initial particle size and quenching, the choice of an inert carrier gas can also affect the pyrolysis evolution. The results show that for efficient quenching processes, the use of nitrogen as a carrier gas can lead to significantly improved tar yields over those obtained with inert steam. This difference in behavior was attributed primarily to differences in the heat capacities of the two gases.

Finally, results from a sensitivity analysis of several thermo-chemical properties of the biomass were presented. Simulations illustrated the sensitivity of tar yields to the apparent density, thermal conductivity, heat capacity and primary heats of reaction. Conversion times were significantly decreased by altering the apparent density from hardwood to softwood measured values due to earlier pyrolysis initialization; however, final tar yields were relatively unchanged in magnitude. The results also suggested that the pyrolysis yields are relatively insensitive to the thermal conductivity and primary heats of reaction. However, a relatively strong sensitivity to the biomass heat capacity was found.

#### ACKNOWLEDGMENTS

This research was conducted at the Jet Propulsion Laboratory (JPL) and sponsored by the U.S. Department of Energy (DOE), with Mr. Neil Rossmcissl (DOE Headquarters) and Mr. D. Hooker (DOE Golden Center) serving as contract monitors, under an agreement with the National Aeronautics and Space Administration. Computational resources are provided by the super computing facility at JPL. The authors wish to thank Dr. Esteban Chornet and Dr. Robert Evans of the National Renewable Energy Laboratory for helpful discussions.

## REFERENCES

Antal, M. J. Biomass pyrolysis: A review of the literature. Part I. Carbohydrate pyrolysis. In K. Bocr and J. Duffie, editors, *Advances in Solar Energy*, pages 61-111. American Solar Energy Society, Boulder, CO, 1982.

Chornet, E., Wang, D., Montane, D., and Czernik, S. Hydrogen production by fast pyrolysis of biomass and catalytic steam reforming of pyrolysis oil. in A. V. Bridgwater, editor, *Advances in thermochemical Biomass Conversion*, volume 1, pages 246-262. Blackie Academic and Professional, New York, New York, 1992.

Chum, H. L., Johnson, D. K., Agblevor, F. A., Evans, R. J., Ilamcs, B. R., Milne, T. A., and Overend, R. P. Status of the IEA voluntary standards activity - Round robins on whole wood and lignins. in A. V. Bridgwater, editor, *Advances in Thermochemical Biomass Conversion*, volume 2, pages 1701-1716. Blackie Academic and Professional, New York, New York, 1992.

DiBlasi, C. Analysis of convection and secondary reaction effects within porous solid fuels undergoing pyrolysis. *Combust. Sci. and Tech.*, 90:315-340, 1993.

DiBlasi, C. Modeling and simulation of combustion processes of charring and non-charring solid fuels. *Prog. Energy Combust. Sci.*, 19:71-104, 1993.

Diebold, J. P. and Power, A. Engineering aspects of the vortex pyrolysis reactor to produce primary pyrolysis oil vapors for use in resins and adhesives. In A. V. Bridgwater and J. L. Kuester, editors, *Research in Thermochemical Biomass Conversion*, pages 609-628. Elsevier Applied Science, New York, New York, 1988.

Koufopoulos, C. A., Papayannakos, N., Maschio, G., and Lucchesi, A. Modelling of the pyrolysis of biomass particles. Studies on kinetics, thermal and heat transfer effects. *Can. J. Chem. Eng.*, 69:907-915, 1991.

Liden, A. G., Berruti, F., and Scott, D. S. A kinetic model for the production of liquids from the flash pyrolysis of biomass. *Chem. Eng. Comm.*, 65:207-221, 1988.

Lirn, K. S., Zhu, J. X., and Grace, J. R. Hydrodynamics of gas-solid fluidization. *Fuel*, 21(Suppl.): 141-193, 1995.

Maschio, G., Lucchesi, A., and Koufopoulos, C. A. Study of kinetic and transfer phenomena in the pyrolysis of biomass particles. In A. V. Bridgwater, editor, *Advances in Thermochemical Biomass Conversion*, volume 2, pages 746-759. Blackie Academic and Professional, New York, New York, 1992.

Miller, R. S. and Bellan, J. Analysis of reaction products and conversion time in the pyrolysis of cellulose and wood particles. *Comb. Sci. Tech.*, 1996. in Press.

Miller, R. S. and Bellan, J. A generalized biomass pyrolysis model based on superimposed cellulose, hemicellulose and lignin kinetics. *Comb. Sci. Tech.*, 1996. Submitted.

Mok, W. S., Antal, M. J., Szabo, P., Varhegyi, G., and Zelci, B. Formation of charcoal from biomass in a scaled reactor. *Ind. Eng. Chem. Res.*, 31:11 62– 1166, 1992.

Narayan, R. and Antal, M. J. Thermal lag, fusion, and the compensation effect during biomass pyrolysis. *Ind. Eng. Chem. Res.*, 35(5): 1711-1721, 1996.

Pyle, D. L. and Zaror, C. A. Heat transfer and kinetics in the low temperature pyrolysis of solids, *Chem. Eng. Sci.*, 39(1):147–158, 1984.

Scott, D. S. and Piskorz, J. The flash pyrolysis of aspen-poplar wood, *Can. J. Chem. Eng.*, 60:666–674, 1982.

Scott, D. S., Piskorz, J., Bergougnou, M. A., Graham, R., and Overend, R. P. The role of temperature in the fast pyrolysis of cellulose and wood. *Ind. Eng. Chem. Res.*, 27:8-15, 1988.

SERI. A survey of biomass gasification: Volume II - Principles of gasification. Technical Report TR-33-239, Solar Energy Research Institute, Golden, Colorado, July 1979.

Thurner, F. and Mann, U. Kinetic investigation of wood pyrolysis, *Ind. Eng. Chem. Process Des. Dev.*, 20:482–488, 1981.

Wagenaar, B. M., Kuipers, J. A. M., Prins, W., and van Swaaij, W. P. M. The rotating cone flash pyrolysis reactor. in A. V. Bridgwater, editor, *Advances in Thermochemical Biomass Conversion*, volume 2, pages 1122-1133. Blackie Academic and Professional, New York, New York, 1992.

Ward, S. M. and Braslaw, J. Experimental weight loss kinetics of wood pyrolysis under vacuum, *Comb. and Flame*, 61:261-269, 1985.

# TABLES

Species	$M [\frac{kg}{kg \cdot mole}]$	$C_v [\frac{kJ}{kg \cdot K}]$	$\mu [\frac{kg}{m \cdot s}]$	$\lambda [\frac{kJ}{m \cdot s \cdot K}]$	$D [E;?]$
$H_2O$	18.016	2.20	$2.9 \times 10^{-5}$	$7.8 \times 10^{-5}$	$1.1 \times 10^{-4}$
$N_2$	28.013	0.8246	$3.58 \times 10^{-5}$	$5.63 \times 10^{-5}$	$8.52 \times 10^{-4}$

Table 1: Property values for steam and nitrogen. Values are for  $T=800K$  and  $p=100kPa$

Biomass	Cellulose	Hemicellulose	Lignin	Source
Beech	0.48	0.28	0.24	Maschio <i>et. al.</i> (1992)
Maple	0.40	0.38	0.22	Mok <i>et. al.</i> (1992)
Oak	0.35	0.40	0.25	SERI (1979)
Olive husk	0.22	0.33	0.45	Maschio <i>et. al.</i> (1992)
Pine	0.50	0.27	0.23	Ward & Braslaw (1985)
Wheat straw	0.42	0.42	0.16	Chum <i>et. al.</i> (1992)

Table 2: Biomass compositions by mass used in this study. All extractive and ash content are included with the hemicellulose.

## FIGURE CAPTIONS

Figure 1: Temporal evolutions of the (a) conversion, and (b) tar collection at the surface ( $R_H/R_{p,0} = 1$ ), for various biomass feedstocks. The particle conditions are;  $R_{p,0} = 0.5cm$  and  $T_R = 900K$ .

Figure 2: Kinetic yield limits as a function of temperature for both char and tar collection with secondary reactions turned off. The solid line is for maple and the dotted is for olive husk.

Figure 3: Temporal evolution of the tar collection obtained from maple at various values of  $R_H/R_{p,0}$ . The particle conditions are;  $R_{p,0} = 0.5cm$  and  $T_R = 900K$ .

Figure 4: Temperature dependence of the (a) char yield, and (b) tar collection at various values of  $R_H/R_{p,0}$ , for both maple and olive husk. The initial particle size is  $R_{p,0} = 0.5cm$ .

Figure 5: Tar collection for maple as a function of the initial particle size for various values of  $T_R$ ; (a)  $R_H/R_{p,0} = 1$ , (b)  $R_H/R_{p,0} = 1.25$ , and (c)  $R_H/R_{p,0} = 1.5$ .

Figure 6: Effects of altering the carrier gas on the pyrolysis of a maple particle with  $R_{p,0} = 0.5cm$  and  $T_R = 900K$ . (a) The mass averaged particle temperature as a function of normalized time. (b) Temporal evolution of the tar collection at various values of  $R_H/R_{p,0}$ .

Figure 7: Temporal evolution of the tar collection at various values of  $R_H/R_{p,0}$  for pine. The initial apparent densities of the biomass are  $\rho_0 = 650kg/m^3$  (solid line) and  $\rho_0 = 450kg/m^3$  (dotted line). The particle conditions are;  $R_{p,0} = 0.5cm$  and  $T_R = 900K$ .

Figure 8: Temporal evolution of the tar collection at  $R_H/R_{p,0} = 1$  for maple; (a) varying the biomass thermal conductivity  $\pm 25\%$ , and (b) varying the biomass heat capacity  $\pm 10\%$ . The particle conditions are  $R_{p,0} = 0.5cm$  and  $T_R = 900K$ , and the base values are  $\lambda_w = 1.256 \times 10^{-4} \frac{kJ}{m \cdot s \cdot K}$  and  $C_w = 2.3 \frac{kJ}{kg \cdot K}$ .

Figure 9: Temporal evolution of the tar collection at  $R_H/R_{p,0} = 1$  for maple; (a) varying the heat of reaction



$\Delta h_2$  by  $\pm 20\%$ , and (b) varying the heat of reaction  $\Delta h_3 \pm 20\%$ . The particle conditions are  $R_{p,0} = 0.5\text{cm}$  and  $T_R = -900\text{K}$ , and the base values for the heats of reaction are  $\Delta h_2 = +255\text{kJ/kg}$  and  $\Delta h_3 = -20\text{kJ/kg}$ .

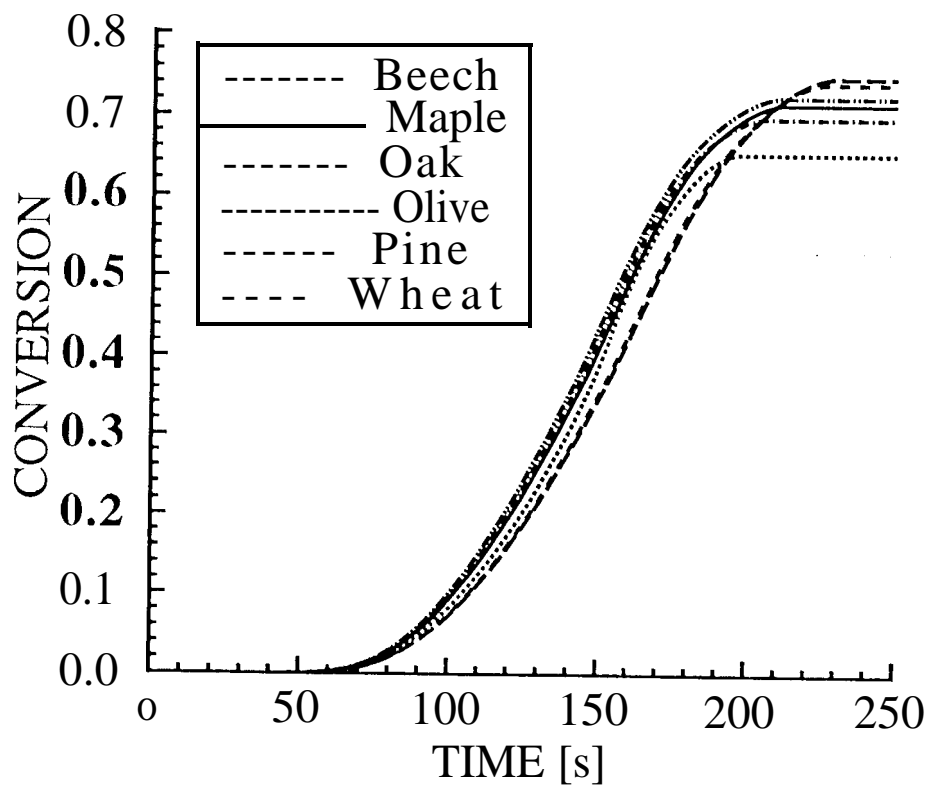


Figure 1 (a)

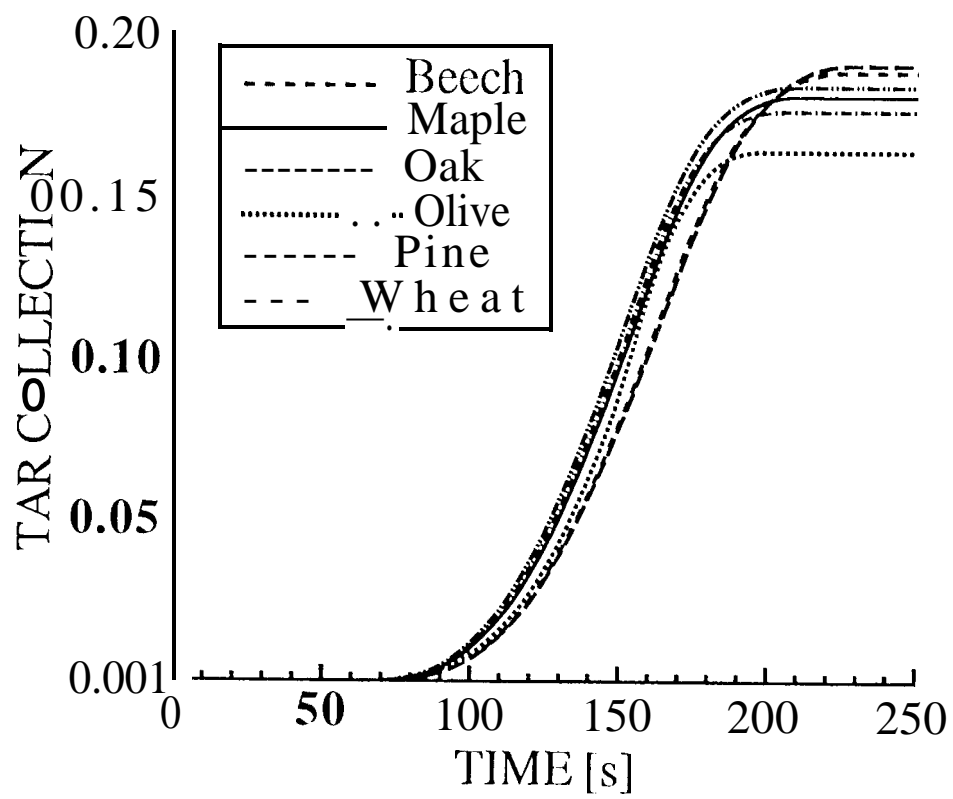


Figure 1 (b)

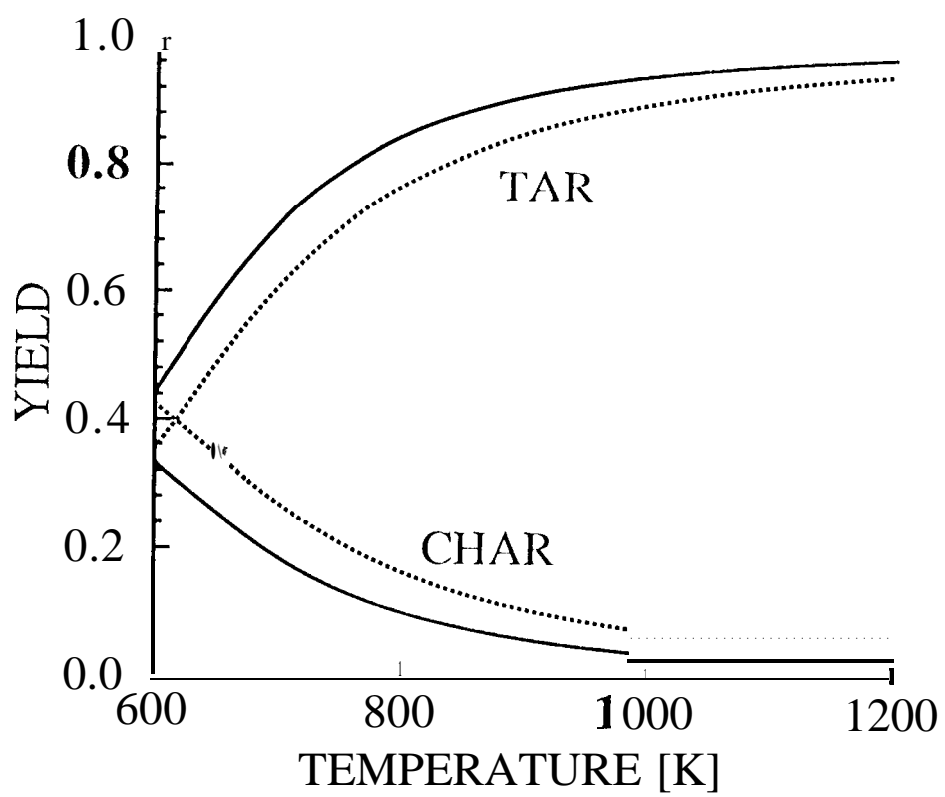


Figure 2

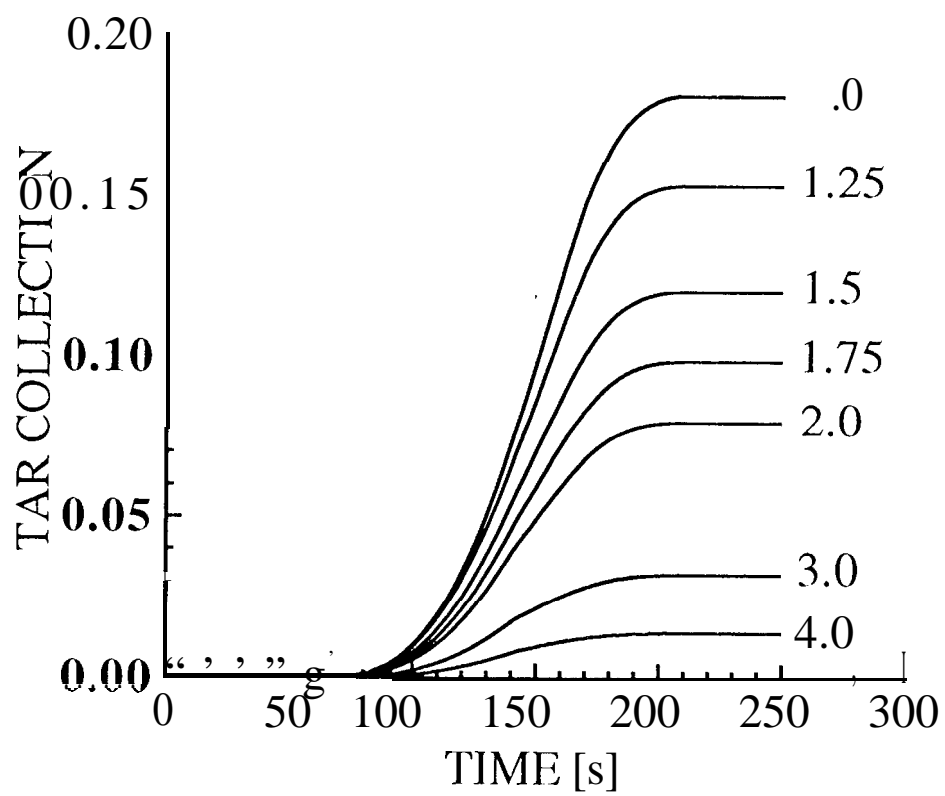


Figure 3

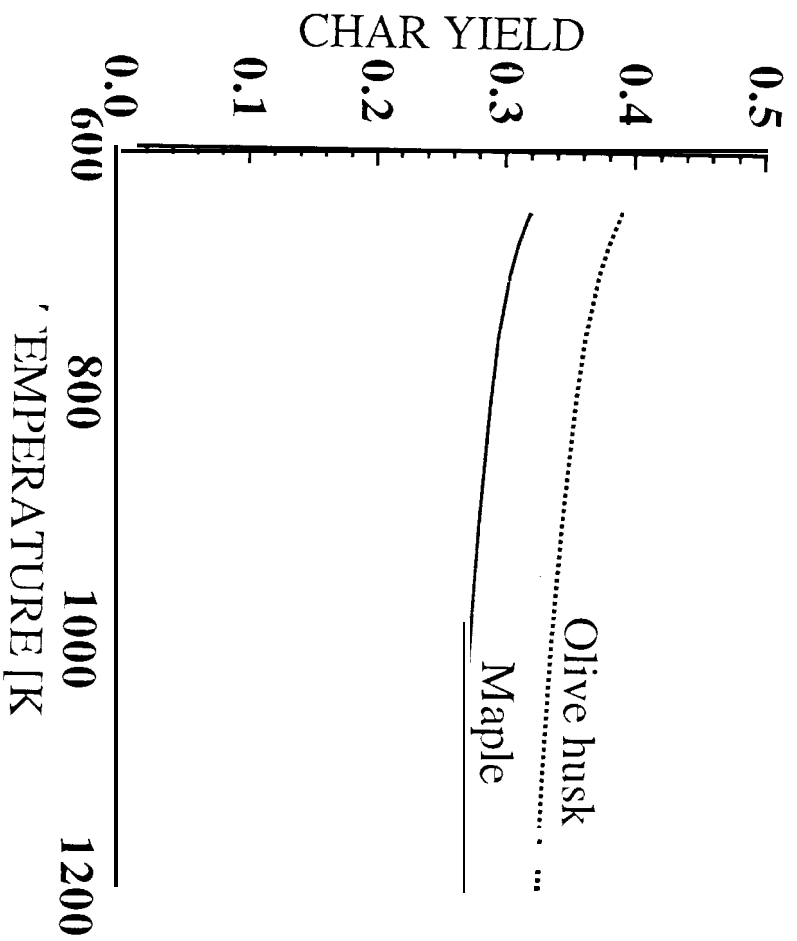


Figure 41(a)

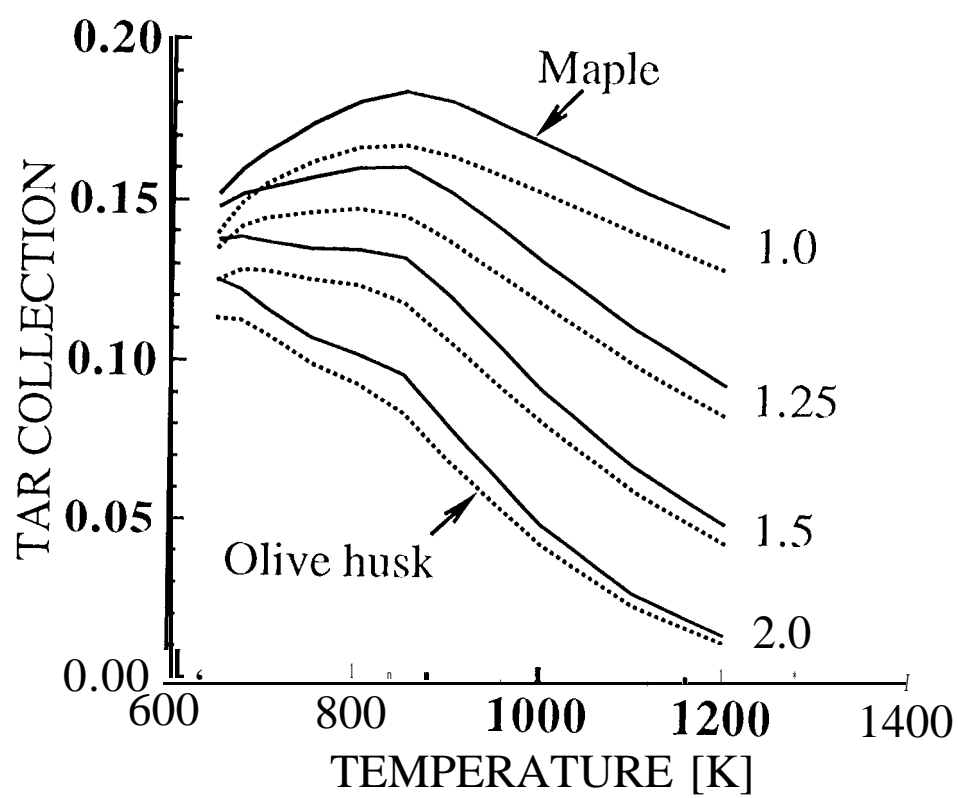


Figure 4(b)

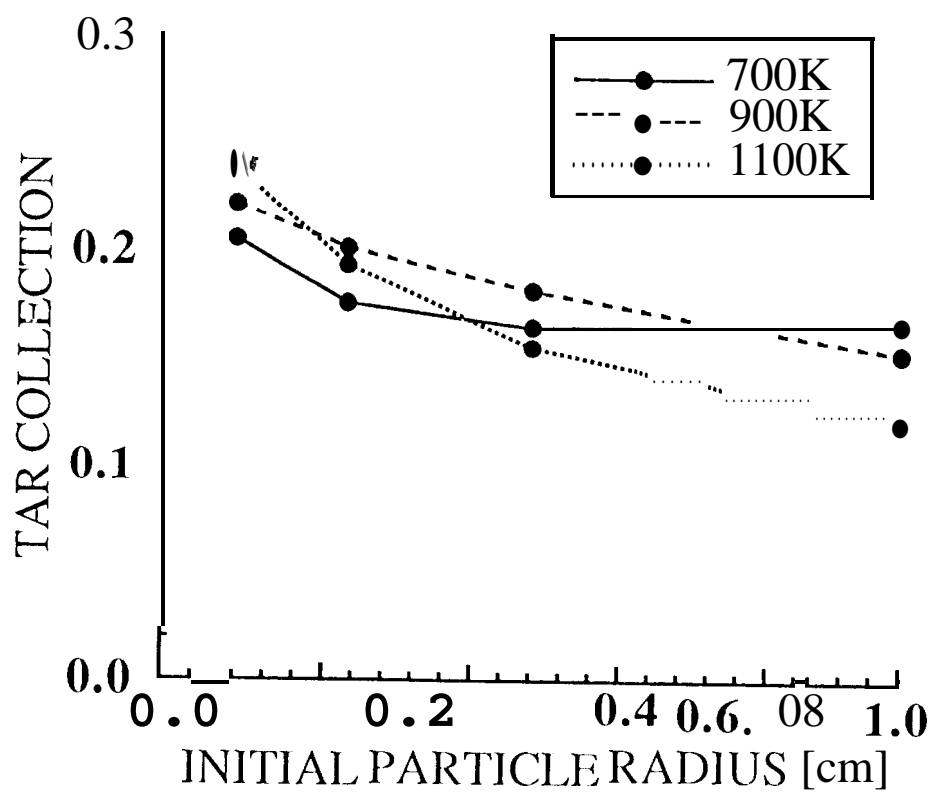


Figure 5 (a)



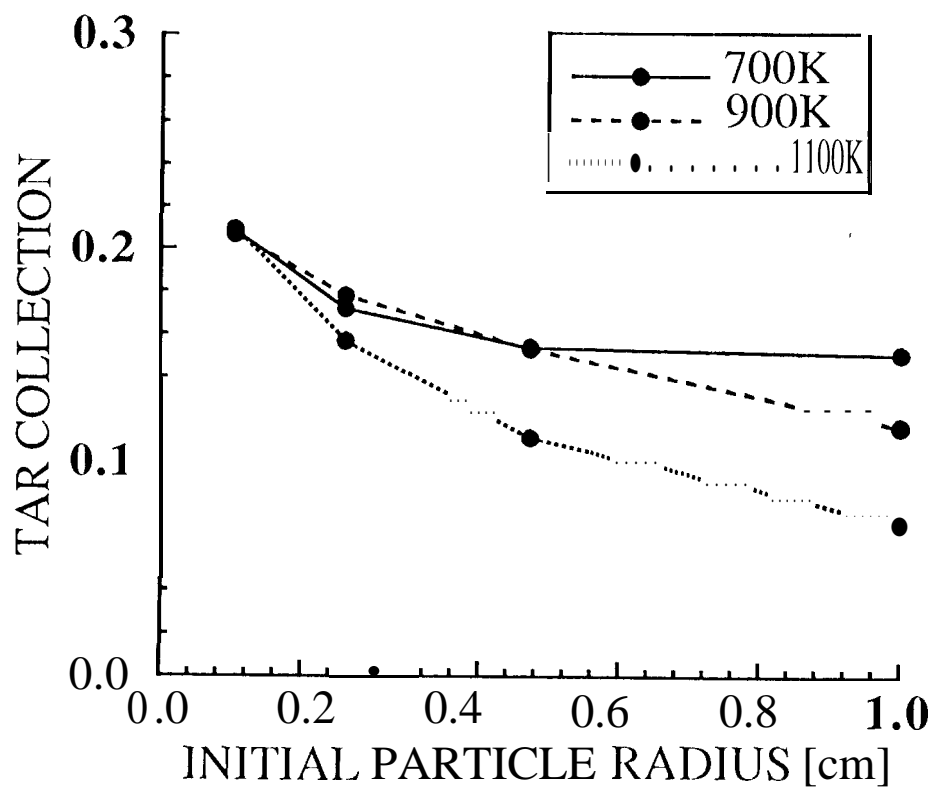


Figure 5(b)

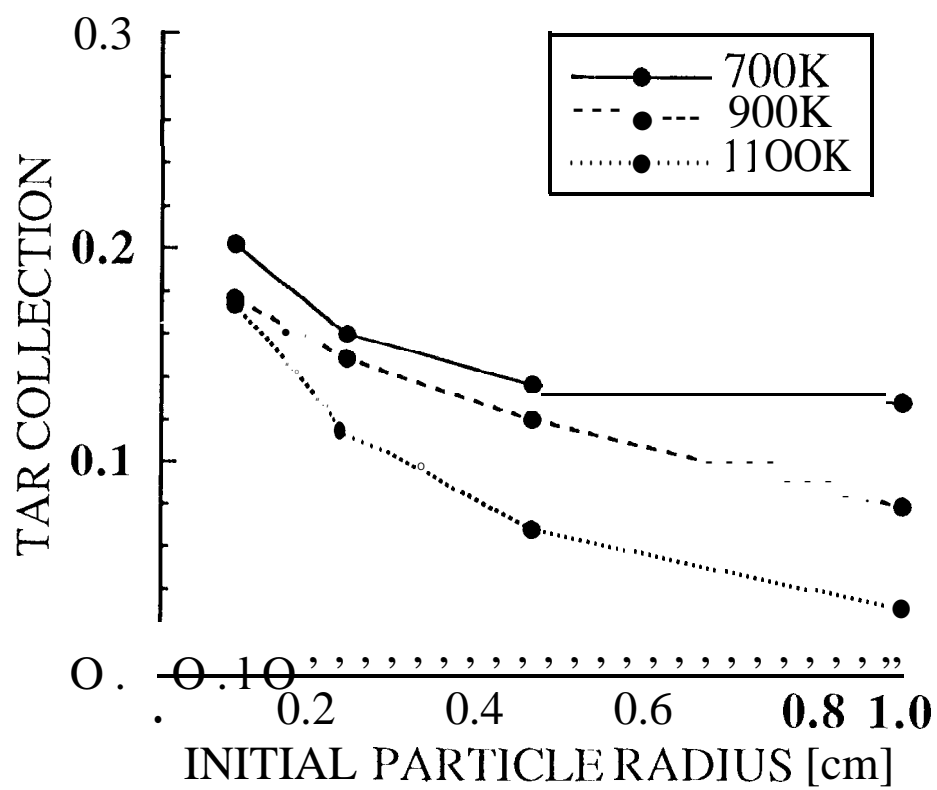


Figure 5(c)

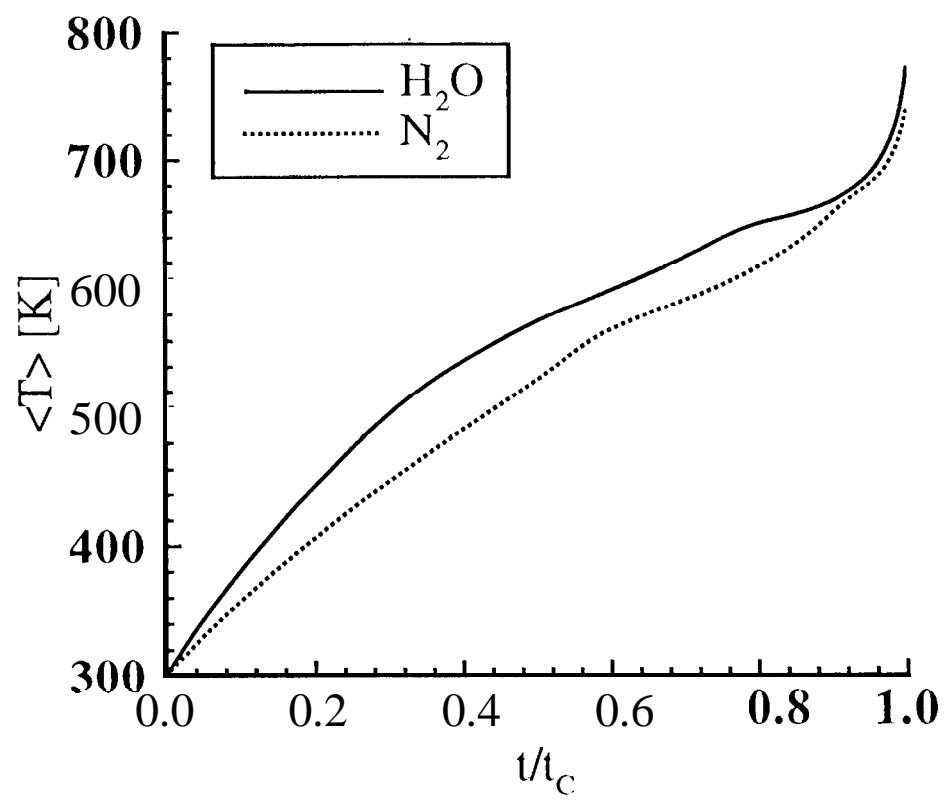


Figure 6(a)

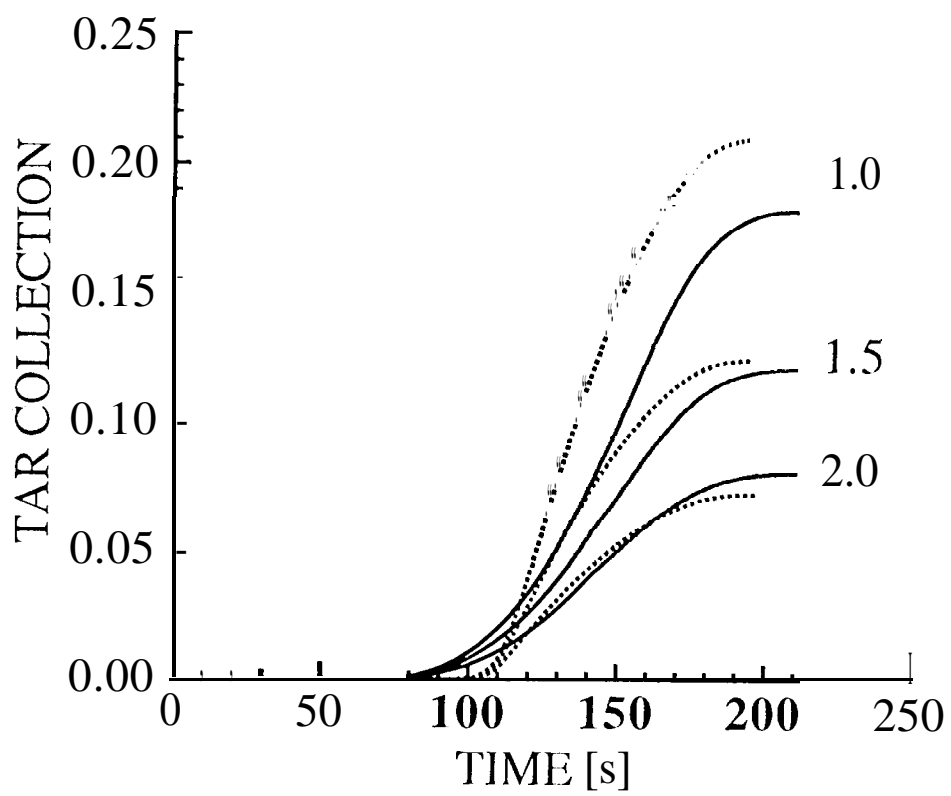


Figure 6(b)

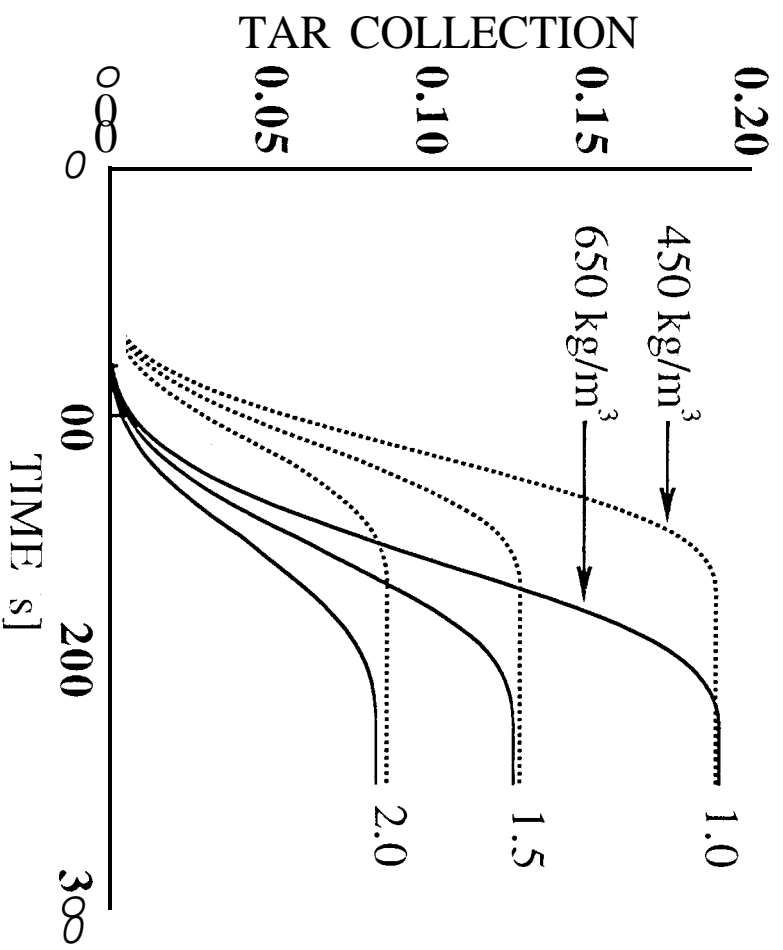


Figure 1

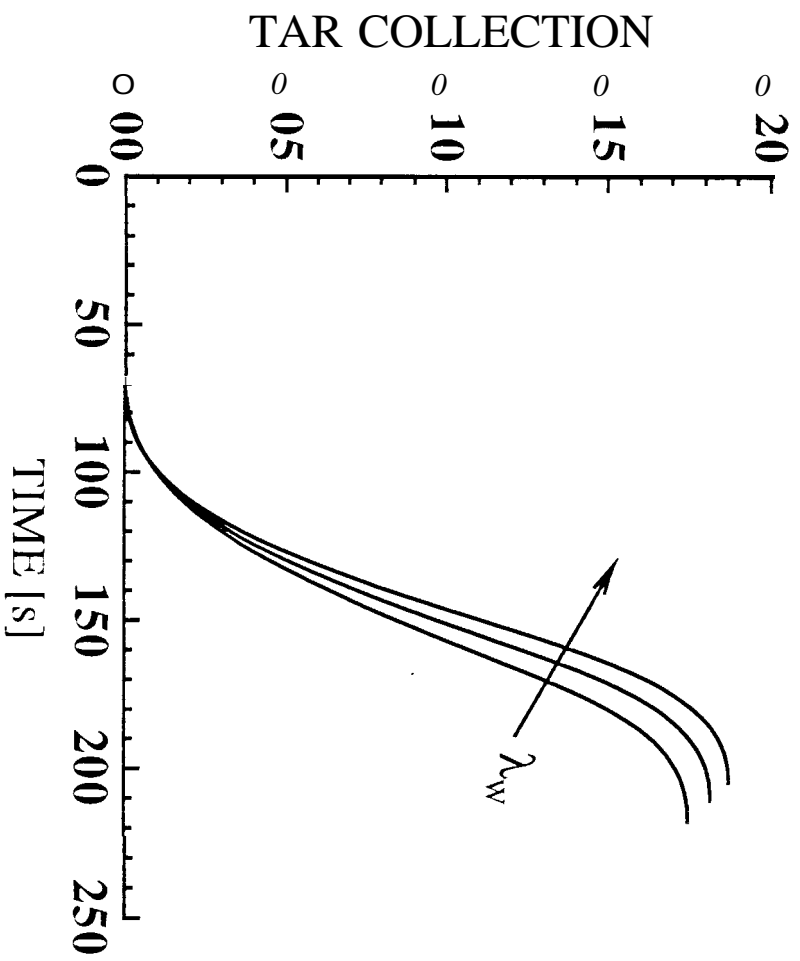


Figure 8(a)

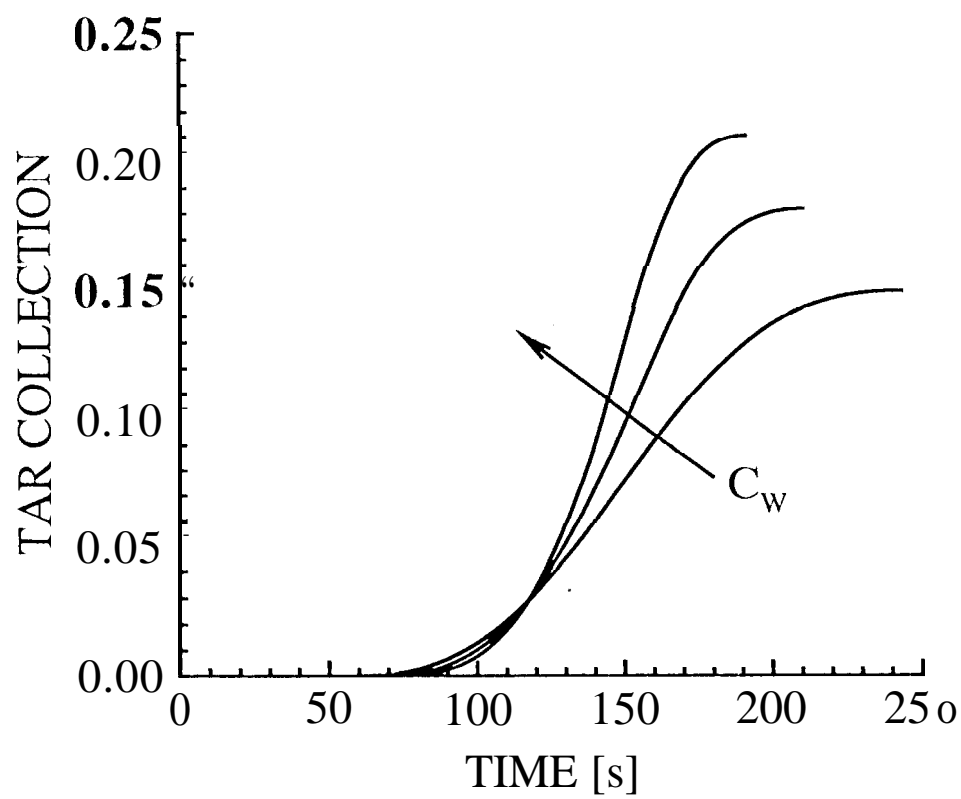


Figure 8(b)

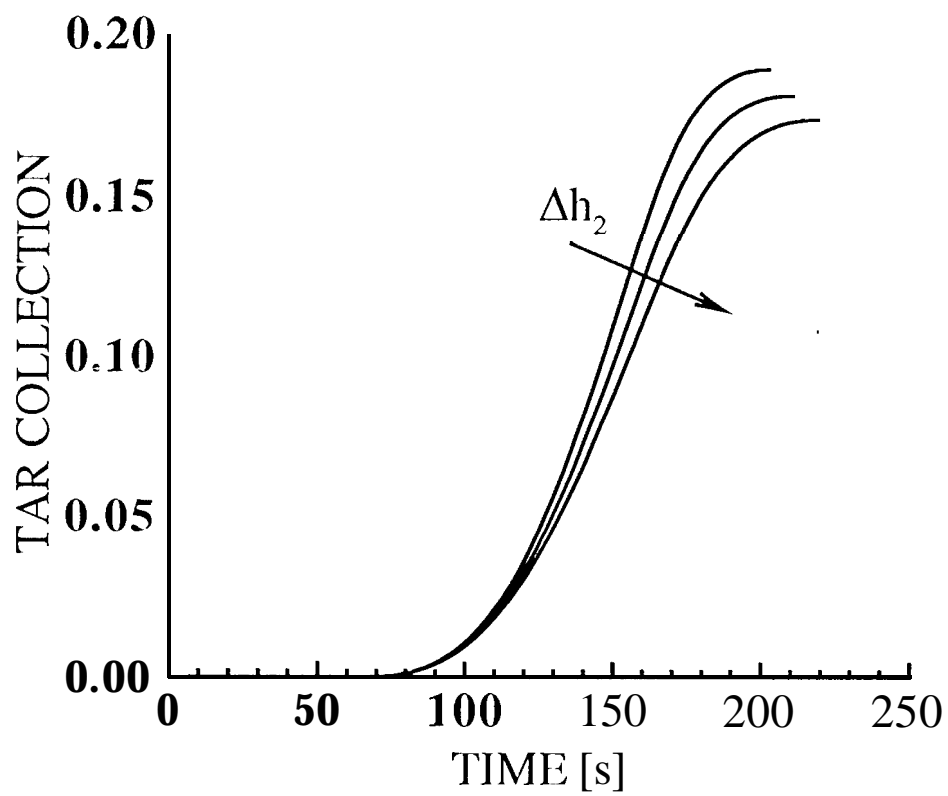


Figure 9 (a)



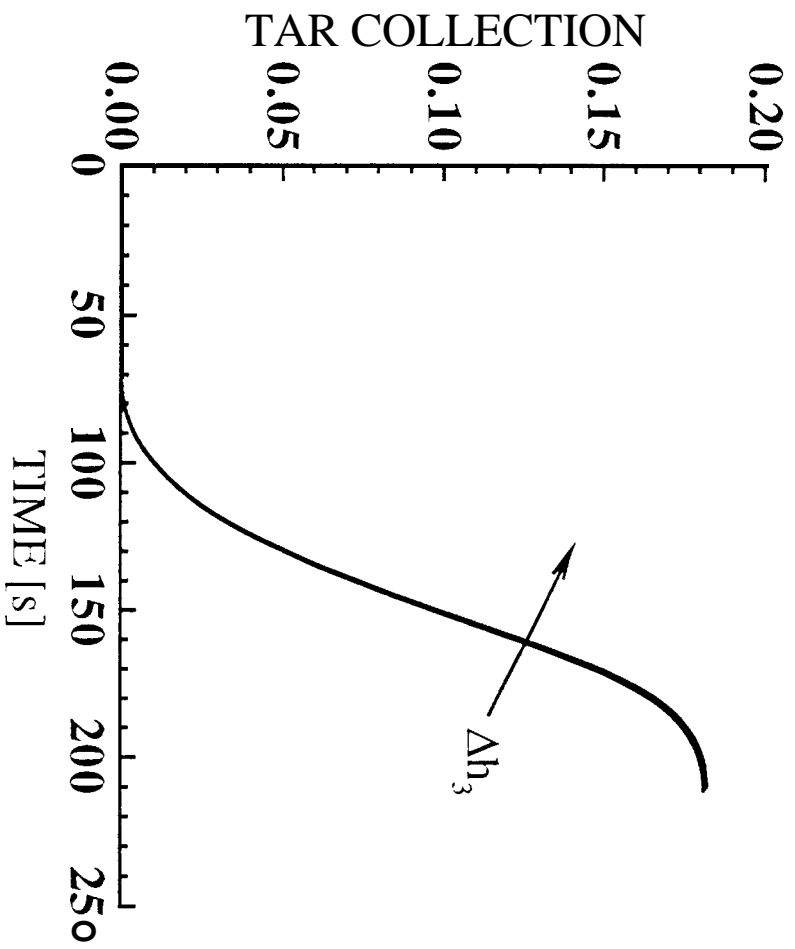


Figure 9(b)